ATLAS PUB Note
ATL-PHYS-PUB-2018-024
29th October 2018

Prospects for a search of invisible particles produced in association with single-top quarks with the ATLAS detector at the HL-LHC

The ATLAS Collaboration

ATL-PHYS-PUB-2018-024
29 October 2018

The expected sensitivity of a search for events with one top quark and large missing transverse momentum is estimated using simulated proton–proton collisions at a centre-of-mass energy of 14 TeV with the ATLAS experiment at the HL-LHC. A non-resonant production of an exotic state decaying to a pair of invisible dark-matter particles in association with a right-handed top quark is considered. Only the topologies where the W boson from the top quark decays into an electron or a muon and a neutrino are considered. Assuming an integrated luminosity of 3000 fb^{-1}, the expected exclusion limit (discovery reach) at 95% CL on the mass of the exotic state is 4.6 TeV (4.0 TeV) using a multivariate analysis based on a boosted decision tree.

1 Introduction

The discovery of a Standard Model (SM) Higgs-like boson in 2012 by the ATLAS [1] and CMS [2] Collaborations opened up new possibilities in searches for new physics. In fact, even with the existence of a Higgs boson confirmed, the SM cannot be considered a complete description of nature. For example, the theory does not explain the fermion generations and mass hierarchy, nor the origin of the matter–antimatter asymmetry in the Universe. Neither does it describe the existence of non light-emitting matter, usually referred to as dark matter (DM), nor describe gravitational interactions. The SM is therefore generally regarded as a low-energy approximation of a more fundamental theory with new degrees of freedom and symmetries that would become manifest at higher energy.

Despite the strong evidence from astrophysical measurements [3–5] which support the existence of DM, there is no evidence yet for non-gravitational interactions between DM and SM particles. DM particles are not expected to interact with the detector and therefore can not be directly detected but can be inferred through a large amount of missing transverse momentum. The specific search strategy depends on what type of particle or system is recoiling against the unseen DM. Both the ATLAS and CMS Collaborations have carried out searches for DM particles produced in association with jets [6–9], photons [10, 11], W or Z [7, 12, 13] and Higgs [14–17] bosons, significantly constraining the allowed parameter space for generic classes of models predicting DM candidates.

This note describes the expected sensitivity of a search for the non-resonant production of an exotic state decaying into a pair of invisible DM particle candidates in association with a right-handed top quark. Such final-state events, commonly referred to as "monotop" events, are expected to have a reasonably small background contribution from SM processes [18]. In this analysis only the topologies where the W boson from the top quark decays into a lepton and a neutrino are considered.

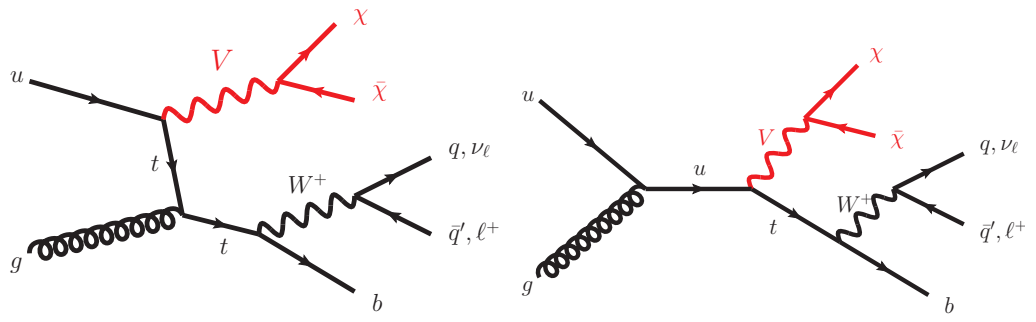

Figure 1: Representative leading-order Feynman diagrams corresponding to the monotop signals searched for non-resonant (a) t- and (b) s-channel DM production in association with a top quark.

The non-resonant monotop production via a flavour-changing neutral interaction is shown in Figure 1 where a top quark (t), a light-flavour up-type quark (u) and an exotic massive vector-like particle V can be parametrised through a general Lagrangian [18, 19]:

$$\mathcal{L}_{\text{int}} = aV_\mu \bar{u}\gamma^\mu P_{\text{R}} t + g_\chi V_\mu \bar{\chi}\gamma^\mu \chi + \text{h.c.}, \tag{1}$$

where V is coupled to a pair of DM particles (represented by Dirac fermions $\chi\bar{\chi}$) whose strength can be controlled through a parameter g_χ and where P_{R} represents the right-handed chirality projector. The

parameter a stands for the coupling constant between the massive invisible vector boson V, and the t- and u-quarks, and γ^μ are the Dirac matrices. A detailed description of further assumptions present in the benchmark models can be found in Refs. [19, 20].

The study presented here is performed with simulated proton–proton (pp) collisions at a centre-of-mass energy of 14 TeV within the framework of the HL-LHC with an upgraded ATLAS detector [21, 22] and assuming an integrated luminosity of 3000 fb^{-1}. Similar searches for such topologies were previously done by the CDF Collaboration in proton–antiproton ($p\bar{p}$) collisions at $\sqrt{s}$ = 1.96 TeV at the Tevatron, using 7.7 fb^{-1} [23], excluding the presence of such vector particles of masses of up to 150 GeV. Using pp collisions at the LHC, the ATLAS Collaboration set a limit of 657 GeV using 20.3 fb^{-1} of pp collision data at $\sqrt{s}$ = 8 TeV [24] and the CMS Collaboration in a search using 36 fb^{-1} at $\sqrt{s}$ = 13 TeV [25], excluded masses up to 2 TeV. This result superseded the previous search by CMS using 19.7 fb^{-1} at $\sqrt{s}$ = 8 TeV [26].

2 Upgraded ATLAS detector at the HL-LHC

The HL-LHC is currently expected to begin its operations in the second half of 2026, with a nominal levelled instantaneous luminosity of 7.5×10^{34} cm^{-2} s^{-1} at $\sqrt{s}$ = 14 TeV. This will lead to an average number of approximately 200 inelastic pp collisions per bunch-crossing (pile-up). This will be significantly higher than the average pile-up of 50 during 2018 data-taking at 2.1×10^{34} cm^{-2} s^{-1}. This programme aims to provide a total integrated luminosity of 3000 fb^{-1} by 2036. Upgrades of the ATLAS detector[1] will be necessary to maintain its performance in the higher luminosity environment and to mitigate the impact of radiation damage and detector ageing. The inner detector will be completely replaced for the HL-LHC, using an all-silicon design (referred to as "ITk") with increased granularity, higher read-out bandwidth and reduced material budget [27, 28]. It will be extended to provide tracking in the region $|\eta| < 4$. The performance of the ITk will be as good, and in most cases better, than the existing inner detector in an environment with significantly higher overlapping events. All of the calorimeters except the forward calorimeters will maintain their current performance and they will not be replaced, although the readout electronics will be replaced to enable improved triggering [29, 30]. A new high-granularity timing detector (HGTD) will also be installed in the forward regions to reduce occupancy from $|\eta| < 2.4$ up to $|\eta| < 4.0$ in the high pile-up HL-LHC environment [31]. The muon detector will be upgraded [32] in order to: extend coverage for muon identification to $|\eta| < 4.0$; permit the use of precision tracking for early trigger decisions; reduce the fake trigger rate in the forward region while preserving high efficiency; and increase trigger acceptance to $|\eta| < 2.7$ by eliminating gaps. The trigger and data acquisition systems will be improved to preserve high signal acceptance in the high-rate and high-occupancy HL-LHC environment [33]. The improvements will include: higher bandwidth readout; using high granularity measurements and tracking information earlier in the trigger. The hardware-based first-level trigger accept rate is planned to be 400-1000 kHz, while the software-based high-level trigger accept rate will be 10 kHz, i.e. an increase of about a factor 10 compared to the high-level trigger at the current ATLAS detector. The b-jet efficiency and light-flavour-quark rejection of the projected ATLAS detector at the HL-LHC is expected to be similar

[1] ATLAS uses a right-handed coordinate system with its origin at the nominal IP in the centre of the detector and the z-axis along the beam pipe. The x-axis points from the IP to the centre of the LHC ring, and the y-axis points upward. Cylindrical coordinates (r, ϕ) are used in the transverse plane, ϕ being the azimuthal angle around the z-axis. The pseudorapidity is defined in terms of the polar angle θ as $\eta = -\ln\tan(\theta/2)$. The transverse momentum and energy are defined as $p_{\mathrm{T}} = p \sin\theta$ and $E_{\mathrm{T}} = E \sin\theta$, respectively. The ΔR is the distance defined as $\Delta R = \sqrt{(\Delta\eta)^2 + (\Delta\phi)^2}$.

to that of the current detector while the c-jet rejection is expected to be about a factor of two lower than that of the current detector [34].

3 Signal and background simulation samples

Samples of events generated using Monte Carlo (MC) simulations were produced using different event generators interfaced to various parton showering (PS) and hadronisation generators. After the event generation step, a fast simulation of the trigger and detector effects was added with the dedicated ATLAS software framework [35]. The trigger, reconstruction and identification efficiencies, the energy and transverse momentum resolution of leptons and jets were computed as a function of their η and p_{T} using full simulation studies assuming an upgrade ATLAS detector [22], and were tabulated in smearing functions which provide parameterised estimates of the ATLAS performance at the HL-LHC. These smearing functions were applied to the truth-level quantities, defined in Section 4. The smearing functions assume the HL-LHC conditions of an instantaneous luminosity of 7.5×10^{34} cm^{-2} s^{-1} and the presence of 200 overlapping events in each bunch-crossing [36]. Detailed studies are shown in Refs. [37, 38].

All the signal and background processes involving top quarks were simulated assuming a top-quark mass of $m_t = 172.5$ GeV and a branching ratio (BR) of 100% for the decay $t \to Wb$. All samples are normalised using their corresponding theoretical production cross-sections.

3.1 Signal samples

For the matrix-element (ME) calculations, samples of signal events generated using the non-resonant monotop model were produced using the MadGraph5_aMC@NLO (v2.3.3) [39] generator at leading-order (LO) using the NNPDF3.0 LO [40] parton distribution function (PDF) set. The PS, hadronisation and the underlying event (UE) were handled by the Pythia 8 (v8.30) event generator [41] with the A14 [42] set of tuned parameters, using the NNPDF2.3 LO PDF set [43]. The EvtGen (v1.6.0) program [44] was used to describe the properties of the bottom and charmed hadron decays. All these MC simulation samples were generated for a range of the mediator masses between $m_V = 1.0$ and 5.0 TeV, in steps of 0.5 TeV. The benchmark DM particle masses are assumed to be $m_\chi = 1$ GeV (larger masses, up to around 100 GeV, can be considered since kinematic distributions predicted by the model do not change as shown in Ref. [25]). The values of the coupling parameter a was set to 0.5 and g_χ was set to 1.0.

3.2 Background samples

Samples of simulated events for background processes include production of single-top quark, top-quark-antiquark pair ($t\bar{t}$), W/Z boson in association with jets, vector-boson pairs, associated production of a $t\bar{t}$ pair and a W/Z boson and single-top quark in association with a Z boson.

Samples of simulated events for $t\bar{t}$ production and electroweak production of single-top quarks in the s-channel, associated tW and t-channel were produced using the next-to-leading-order (NLO) Powheg-Box generator [45–47]. In the $t\bar{t}$ event generation the resummation damping factor[2] was set to $1.5 \times m_t$ and in

[2] The resummation damping factor is one of the parameters controlling the ME/PS matching in Powheg and effectively regulates the high-p_{T} gluon radiation.

the t-channel event generation the four-flavour scheme was used, treating the b-quark as massive. For $t\bar{t}$ and s-channel the NNPDF3.0 NLO PDF set was used in the ME generation, while NNPDF3.04f NLO PDF set was used for the t-channel, and CT10 [48] PDF set for the associated tW process. All these simulation samples except the latter were interfaced to Pythia 8 for the PS, fragmentation and the UE simulation, using the A14 set of tuned parameters and the NNPDF2.3 LO PDF set. The associated tW production sample was interfaced to Pythia 6 [49], using the CT10 PDF set and the corresponding Perugia 2012 tuneable parameters [50].

The W boson production in association with jets was produced using the MadGraph5_aMC@NLO generator at LO using the NNPDF3.0 NLO PDF set. These W+jets event samples were simulated for up to one additional parton at NLO and up to two additional partons at LO. The Z boson production in association with jets (Z+jets) was produced using the Powheg-Box generator at NLO in QCD with the CT10 PDF set and the AZNLO [51] set of tuned parameters of the UE are used. The final-state photon radiation was modelled by the Photos [52] MC simulation. Both productions were interfaced with Pythia 8 generator for the PS, fragmentation and UE, using the CT10 PDF set in the case of W+jets and CTEQ6L1 [53] PDF set in the case of Z+jets.

Samples of vector-boson pairs events (WW, ZZ, WZ), containing up to three additional partons where at least one of the bosons decays leptonically, were produced using the Sherpa generator [54] with the NNPDF3.0 NNLO PDF set.

The associated productions of a $t\bar{t}$ pair and either a W or Z boson ($t\bar{t}W$, $t\bar{t}Z$) were generated using MadGraph5_aMC@NLO at NLO using the NNPDF3.0 NLO [40] PDF set. The generated events were then processed with Pythia 8 to perform the fragmentation and hadronisation, and to generate the UE, using the NNPDF2.3 LO PDF set and the A14 set of tuned parameters.

Samples of single-top quark production in association with a Z boson events (tZq) were generated at LO in QCD using MadGraph5_aMC@NLO in the four-flavour scheme with the CTEQ6L1 LO PDF set. The Z boson was simulated to be on-shell and off-shell Z/γ^* contributions and their interference were not taken into account. The PS, hadronisation and the UE were generated by Pythia 8 with the A14 set of tuned parameters using the NNPDF2.3 LO PDF set.

In all background samples where Pythia 6 or Pythia 8 were used, the EvtGen program was also used to model bottom and charmed hadron decays.

4 Object definition

Particle-level definitions are used for electrons, muons, jets and missing transverse momentum, which are the final-state objects used by this analysis. These are constructed from stable particles of the MC event record with a lifetime larger than 0.3×10^{-10} s within the observable pseudorapidity range.

Electrons and muons, hereafter referred to as leptons (ℓ), need to originate from a W boson, including from an intermediate tau decay. Leptons from hadron decays, either directly or via a tau decay, are rejected. Leptons are requested to have $|\eta| < 2.5$. The selected lepton four-momentum is calculated including photons within a cone of size of $\Delta R = 0.1$. In order to simulate the electron/muon track match requirement (i.e. the overlap removal between electrons and muons), events are rejected if a matching in ϕ and θ of 0.005 is found between these two particle-level objects. Identification efficiencies [22] are applied to the

lepton candidates to select which particles are identified as leptons. These have their energy, p_{T} and η smeared according to the detector resolution.

Neutrinos are required, similarly to electrons and muons, not to originate from a hadron or quark decay. The missing transverse momentum, with magnitude $E_{\mathrm{T}}^{\mathrm{miss}}$, is calculated from the negative vector sum of true final-state particles within the detector acceptance. The contribution due to pile-up is taken into account before applying detector resolution effects.

Jets are reconstructed using the anti-k_t algorithm [55] implemented in the FastJet [56] library, with a radius parameter of 0.4. All stable final-state particles are used to reconstruct the jets, except the selected neutrinos, leptons and the photons associated with these leptons. This implies that the b-jet energy is close to that of the b-quark before hadronisation and fragmentation. The b-tagging is performed if the jet is within $|\eta| < 2.5$ applying a tagging efficiency, function of the true flavour of the jet, p_{T} and η. Since the b-tagging is particularly sensitive to the contamination of pile-up tracks, tracks with large impact parameters are considered. Therefore tracks from nearby pile-up are likely to be selected in order to mitigate effects from pile-up. These efficiencies are evaluated considering the latest layout of the ITk detector [28] though not the HGTD, pile-up of 200 and using the MV2 b-tagging algorithm [34, 57, 58] at the 70% working point. Double counting of electrons as jets may arise from electron energy deposition in the calorimeter being clustered by the jet algorithm. To mitigate such effect jets are removed if within $\Delta R = 0.2$ from a selected electron. After this step, electrons within $\Delta R = 0.4$ from a jet are rejected, since they are considered as decay products of the hadrons in the jet. For the same reason, muons that are within $\Delta R(\mathrm{muon}, \mathrm{jet}) = 0.04 + 10\ \mathrm{GeV}/p_{\mathrm{T}}(\mathrm{muon})$ from a jet are also removed. A fraction of the particle-level jets are removed, according to the expected mis-identification rate shown in Ref. [37]. Energy, p_{T} and η of remaining jets are smeared according to the detector resolution. Pile-up jets are rejected using tracking information.

5 Event selection and analysis strategy

The experimental signature of the non-resonant monotop events with W boson decaying leptonically is one lepton from the W-boson decay, large $E_{\mathrm{T}}^{\mathrm{miss}}$, and one jet identified as likely to be originated from a b-quark. The signal event candidates are selected by requiring exactly one lepton with $p_{\mathrm{T}} > 30$ GeV, exactly one jet with $p_{\mathrm{T}} > 30$ GeV identified as a b-jet and $E_{\mathrm{T}}^{\mathrm{miss}} > 100$ GeV. Since the considered monotop process favours final states with positive leptons, events with negative lepton charge are rejected. These criteria defines the base selection.

In order to maximise the sensitivity of the study, in addition to the base selection further discrimination is achieved by applying additional criteria according to the kinematic properties of the signal while rejecting background. Events entering the pre-selection region defined in Section 5.1 are used to train a boosted decision tree (BDT) algorithm. A selection on the BDT output is used to define the BDT-based signal region. A study was performed to optimise a cut-based analysis and signal region, but it was found to be less effective than a multivariate analysis approach. The results of this study are also described in this Section 5.2. To extract exclusion limits the $E_{\mathrm{T}}^{\mathrm{miss}}$ distribution is used as the discriminating variable when executing the statistical analysis.

5.1 BDT-based analysis

In addition to the base selection, further discrimination between the monotop signal events and background events is achieved by applying additional criteria. The transverse mass of the lepton–$E_{\mathrm{T}}^{\mathrm{miss}}$ system,

$$m_{\mathrm{T}}(\ell, E_{\mathrm{T}}^{\mathrm{miss}}) = \sqrt{2p_{\mathrm{T}}(\ell)E_{\mathrm{T}}^{\mathrm{miss}}\left(1 - \cos\Delta\phi(\ell, E_{\mathrm{T}}^{\mathrm{miss}})\right)}, \tag{2}$$

where $p_{\mathrm{T}}(\ell)$ denotes the magnitude of the lepton transverse momentum and $\Delta\phi(\ell, E_{\mathrm{T}}^{\mathrm{miss}})$ is the azimuthal difference between the lepton momentum and the $E_{\mathrm{T}}^{\mathrm{miss}}$ directions, is required to be larger than 100 GeV in order to reduce the background contribution. In background events the spectrum of this quantity decreases rapidly for values higher than the W-boson mass. In signal events instead, the spectrum has a tail at higher mass values, as seen in the search performed by ATLAS at $\sqrt{s} = 8$ TeV [24]. When originating from the decay of a top quark, the lepton and the b-jet are close to each other. Therefore, events are required to have an azimuthal difference between the lepton momentum and the b-jet momentum directions ($|\Delta\phi(\ell, b\text{-jet})|$) of less than 2.0, which disfavours the W+ jets and diboson backgrounds. Table 1 shows a summary of the previous criteria which defines the pre-selection region. Figure 2 shows the distributions of $|\Delta\phi(\ell, b\text{-jet})|$, the angular distance between the lepton and the b-jet ($\Delta R(\ell, b\text{-jet})$), and $m_{\mathrm{T}}(\ell, E_{\mathrm{T}}^{\mathrm{miss}})$.

Variable	Requirement
Multiplicity (leptons)	1
$p_{\mathrm{T}}(\ell)$ [GeV]	> 30
Lepton charge sign	> 0
$p_{\mathrm{T}}(b\text{-jet})$ [GeV]	> 30
$E_{\mathrm{T}}^{\mathrm{miss}}$ [GeV]	> 100
Multiplicity (b-jets)	1
$m_{\mathrm{T}}(\ell, E_{\mathrm{T}}^{\mathrm{miss}})$ [GeV]	> 100
$\lvert\Delta\phi(\ell, b\text{-jet})\rvert$	< 2.0

Table 1: Overview of the pre-selection criteria used to define the pre-selection region.

Further selection is performed via a BDT algorithm provided by the Toolkit for Multivariate Analysis [59]. The BDT is trained to discriminate the monotop signal from the dominant $t\bar{t}$ background. For the training, since no significant difference is observed for the different mass values, the sample with $m_V = 2.5$ TeV is used. Half of the events of both signal and background samples are selected randomly and used to train the BDT. The other half is used to probe the BDT behaviour in order to avoid the presence of overtraining. The variables entering the BDT are selected from a pool of fundamental quantities, like p_{T} of jets and b-jets, and angular distances. The variables selected are the ones showing the best discriminating power. In particular, $|\Delta\phi(\ell, b\text{-jet})|$ and $m_{\mathrm{T}}(\ell, E_{\mathrm{T}}^{\mathrm{miss}})$ are found to be the most effective variables. A full list and description of the variables used in the BDT training is given in Table 2. Figure 3 shows the distribution of the BDT response in the pre-selection region. Only events with BDT response > 0.9 and $E_{\mathrm{T}}^{\mathrm{miss}} > 150$ GeV enter in the signal region and are used in the extraction of the result. This value is chosen because it maximises the significance while leaving sufficient statistics for the result to be meaningful.

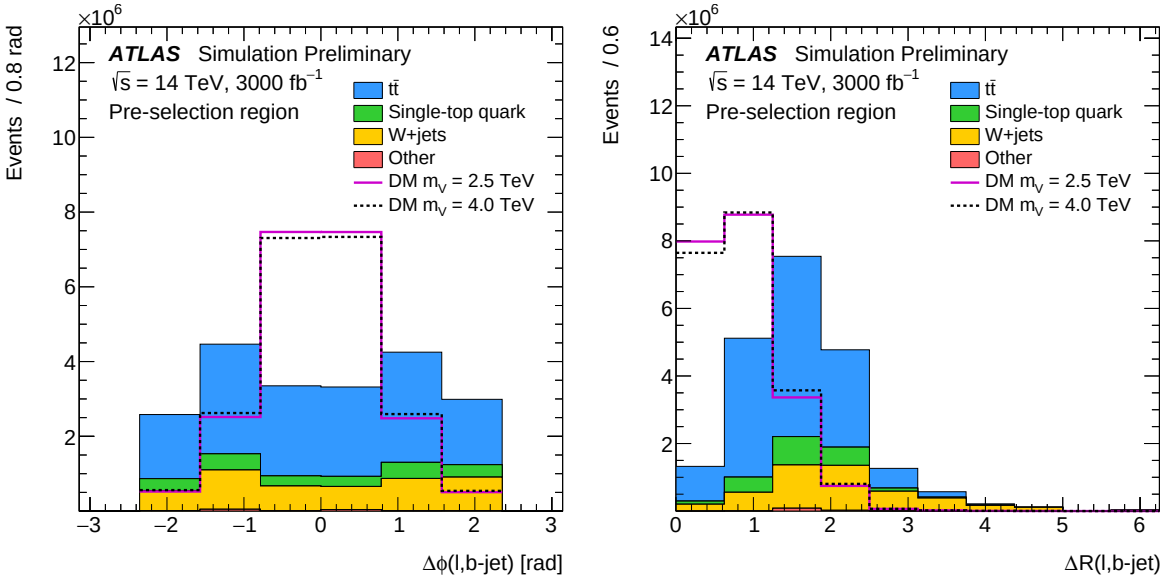

(a) (b)

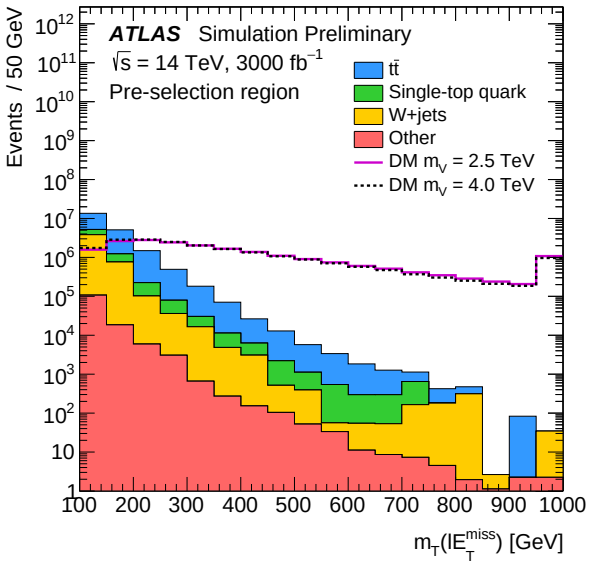

(c)

Figure 2: Distributions of (a) $\Delta\phi$ between the lepton and the b-jet, (b) ΔR between the lepton and the b-jet and (c) transverse mass of the lepton–$E_{\mathrm{T}}^{\mathrm{miss}}$ system. The stack distribution shows the background prediction which includes $t\bar{t}$, single-top quark, W+jets and Other (i.e. Z+jets, dibosons, $t\bar{t}W/Z$ and tZq). Solid and dashed lines represent the signal corresponding to a mediator mass of 2.5 and 4.0 TeV, respectively. The background event samples are normalised to their theoretical predictions and the signal event samples are normalised to the number of background events.

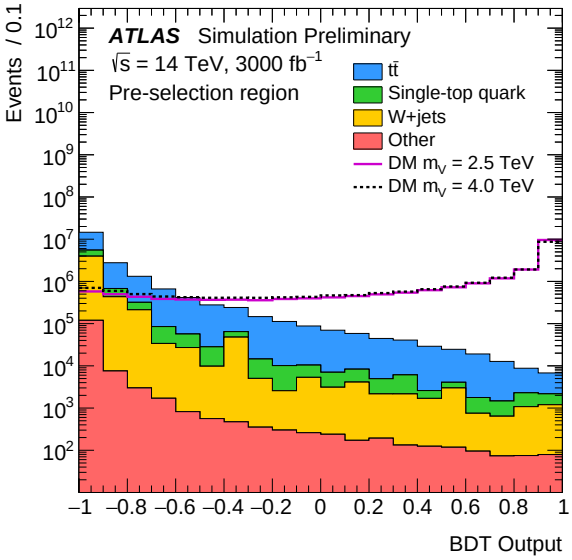

Figure 3: Response of the BDT algorithm for events in the pre-selection region. The stack distribution shows the background prediction which includes $t\bar{t}$, single-top quark, W+jets and Other (i.e. Z+jets, dibosons, $t\bar{t}W/Z$ and tZq). Solid and dashed lines represent the signal corresponding to a mediator mass of 2.5 and 4.0 TeV, respectively. The background event samples are normalised to their theoretical predictions and the signal event samples are normalised to the number of background events.

5.2 Cut-based analysis

Events used in this study are selected with the base selection together with additional requirements in three variables properly optimised. The optimisation is performed by varying systematically the thresholds of $|\Delta\phi(\ell, b\text{-jet})|$, $\Delta R(\ell, b\text{-jet})$ and $m_{\mathrm{T}}(\ell, E_{\mathrm{T}}^{\mathrm{miss}})$, and without taking into account systematics uncertainties. The $E_{\mathrm{T}}^{\mathrm{miss}}$ is used as discriminant variable in the likelihood fit. The tested selection on $m_{\mathrm{T}}(\ell, E_{\mathrm{T}}^{\mathrm{miss}})$ ranges between > 50 GeV and > 300 GeV in steps of 25 GeV. Selections on the angular variables range from < 0.5 to < 2.9, in steps of 0.2. The figure of merit used in this process is the excluded signal strength obtained from the likelihood fit. The fitting procedure is described in Section 6. The signal with $m_V = 2.5$ TeV is used for this study. The optimal set of requirements is found to be the base-section criteria with $\Delta R(\ell, b\text{-jet}) < 1.2$ and $m_{\mathrm{T}}(\ell, E_{\mathrm{T}}^{\mathrm{miss}}) > 225$ GeV and with no requirements on $|\Delta\phi(\ell, b\text{-jet})|$. Additionally a cut on $E_{\mathrm{T}}^{\mathrm{miss}} > 150$ GeV is applied to further reduce background. These criteria define the signal region of the cut-based analysis.

Table 3 shows the predicted event yields in the pre-selection region and in the signal regions of the BDT- and cut-based analyses. Comparing the two signal regions, the former analysis has about two order of magnitude larger signal-to-background ratios than the latter analysis. In both analyses the dominant background is the $t\bar{t}$ production. In the BDT-based analysis, the $t\bar{t}$ background represents the 65% of the total background, followed by an important contribution of W+jets and single top-quark backgrounds. In the cut-based analysis, the $t\bar{t}$ background represents the 90% of the total background with minor contribution of single top-quark production and negligible contribution of the rest.

Variable name	Description
Kinematic variables	
$E_{\mathrm{T}}^{\mathrm{miss}}$	Magnitude of the missing transverse momentum
$p_{\mathrm{T}}(b\text{-jet})$	Transverse momentum of the b-jet
$p_{\mathrm{T}}(\text{leading-jet})$	Transverse momentum of the leading jet
Lepton p_{T}	Transverse momentum of the lepton
$m_{\mathrm{T}}(\ell, E_{\mathrm{T}}^{\mathrm{miss}})$	Transverse mass of lepton–$E_{\mathrm{T}}^{\mathrm{miss}}$ system
Azimuthal differences	
$\lvert\Delta\phi(\ell, \text{leading-jet})\rvert$	$\Delta\phi$ between the lepton and the leading jet
$\lvert\Delta\phi(\ell, b\text{-jet})\rvert$	$\Delta\phi$ between the lepton and the b-jet
$\Delta\phi(\ell, E_{\mathrm{T}}^{\mathrm{miss}})$	$\Delta\phi$ between the lepton and $E_{\mathrm{T}}^{\mathrm{miss}}$
Angular distance differences	
$\Delta R(\ell, \text{leading-jet})$	ΔR between the lepton and the leading jet
$\Delta R(\ell, b\text{-jet})$	ΔR between the lepton and b-jet
Masses	
Leading-jet mass	Mass of the leading jet

Table 2: List of variables entering the BDT and their definitions.

Process	Pre-selection region	Signal region (BDT-based)	Signal region (Cut-based)
m_V = 1.0 TeV	183100 ± 400	58900 ± 200	100300 ± 300
m_V = 1.5 TeV	33700 ± 180	13000 ± 110	19800 ± 140
m_V = 2.0 TeV	8400 ± 90	3530 ± 60	5110 ± 70
m_V = 2.5 TeV	2540 ± 50	1100 ± 30	1560 ± 40
m_V = 3.0 TeV	890 ± 30	380 ± 19	540 ± 20
m_V = 3.5 TeV	360 ± 19	150 ± 12	220 ± 15
m_V = 4.0 TeV	160 ± 13	64 ± 8	97 ± 10
m_V = 4.5 TeV	83 ± 9	31 ± 6	48 ± 7
m_V = 5.0 TeV	47 ± 7	17 ± 4	27 ± 5
Single-top quark	2058000 ± 1400	490 ± 20	32600 ± 180
$t\bar{t}$	14146000 ± 4000	2270 ± 50	407500 ± 600
W+ jets	4617000 ± 2000	710 ± 30	16900 ± 130
Other	136000 ± 400	57 ± 8	1260 ± 40
Total background	20957000 ± 5000	3520 ± 60	458300 ± 700

Table 3: Predicted pre-fit event yields for the merged electron and muon channels in the pre-selection region and for the signal regions of the BDT- and cut-based analyses. The signal and backgrounds are normalised to their theoretical predictions. The uncertainties shown are statistical only.

6 Results

The BDT-based approach is selected given the significantly better results obtained compared to the cut-based analysis. Thus, unless explicitly stated, the content on this section refers to the BDT-analysis.

For the statistical analysis all backgrounds except the $t\bar{t}$ production are merged in a non-$t\bar{t}$ background to avoid problems of poor statistics in the signal region. This allows to use a binned likelihood fit. The shape of the $E_{\mathrm{T}}^{\mathrm{miss}}$ distribution is used in the statistical analysis, as it is expected to be the most sensitive variable to the presence of new physics. The binning of this distribution is optimised for the sensitivity of the analysis in the signal region while ensuring the stability of the fit. This results in a non-equidistant binning which exhibits wider bins in regions with a large signal contribution, while preserving a sufficiently large number of background events in each bin. Figure 4 shows the post-fit $E_{\mathrm{T}}^{\mathrm{miss}}$ distribution in the signal region. The result does not include MC statistical uncertainties but incorporates effects of systematic uncertainties. The theoretical modelling of signal and background has the largest prior, 15%. The second largest source of uncertainty is the one relative to the $E_{\mathrm{T}}^{\mathrm{miss}}$ reconstruction, with 6% prior. Jet energy scale (JES) and jet energy resolution (JER) contribute with a total of 5%. The uncertainty on the requirements for pile-up jets rejection is 5%. The ones on lepton identification and b-tagging efficiencies are 1.2% and 2.5%, respectively. The uncertainty on the expected luminosity is also taken into account, with a 1% effect.

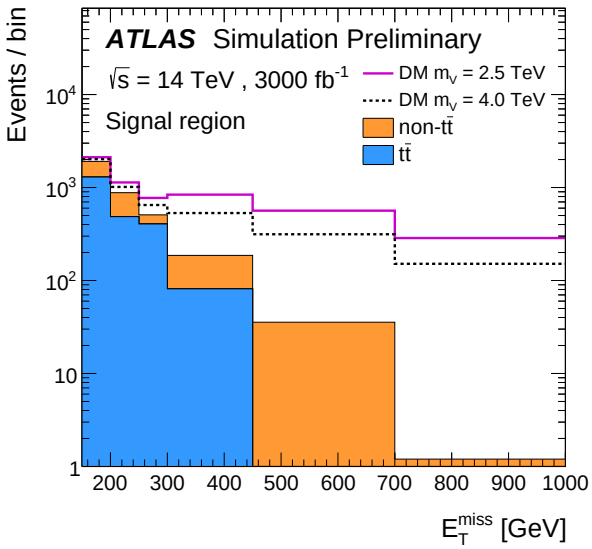

Figure 4: Expected post-fit $E_{\mathrm{T}}^{\mathrm{miss}}$ distribution in the signal region. The stack distribution shows the $t\bar{t}$ and non-$t\bar{t}$ background predictions. Solid and dashed lines represent the signal corresponding to a mediator mass of 2.5 and 4.0 TeV, respectively. The signal event samples are normalised to the number of background events. The binning is the same as the optimised, non-equidistant binning used in the fit. Last bin includes overflow events.

Hypothesis testing is performed using a frequentist approach which uses the asymptotic approximation described in Ref. [60]. Figure 5 shows the expected 95% confidence level (CL) upper limits as a function of the mediator mass for the non-resonant model assuming $m_\chi = 1$ GeV, $a = 0.5$ and $g_\chi = 1$. After the fit, the largest impact on the result is coming from the uncertainty on the $E_{\mathrm{T}}^{\mathrm{miss}}$ reconstruction. This is expected since the $E_{\mathrm{T}}^{\mathrm{miss}}$ is the final discriminant in the analysis. The second largest contribution is coming from background and signal modelling. The other contributions are, in order of importance: pile-up jet rejection requirements, JES and JER, lepton reconstruction efficiency and b-tagging efficiency. The uncertainty

on the expected luminosity is found to have the smallest effect. The expected mass limit at 95% CL is 4.6 TeV while the discovery reach (based on 5σ significance) is 4.0 TeV. For the current analysis the effect of possible improvements in the systematic uncertainties is estimated by reducing by half the uncertainties. This has the effect of increasing the exclusion limit (discovery reach) by 80 (50) GeV.

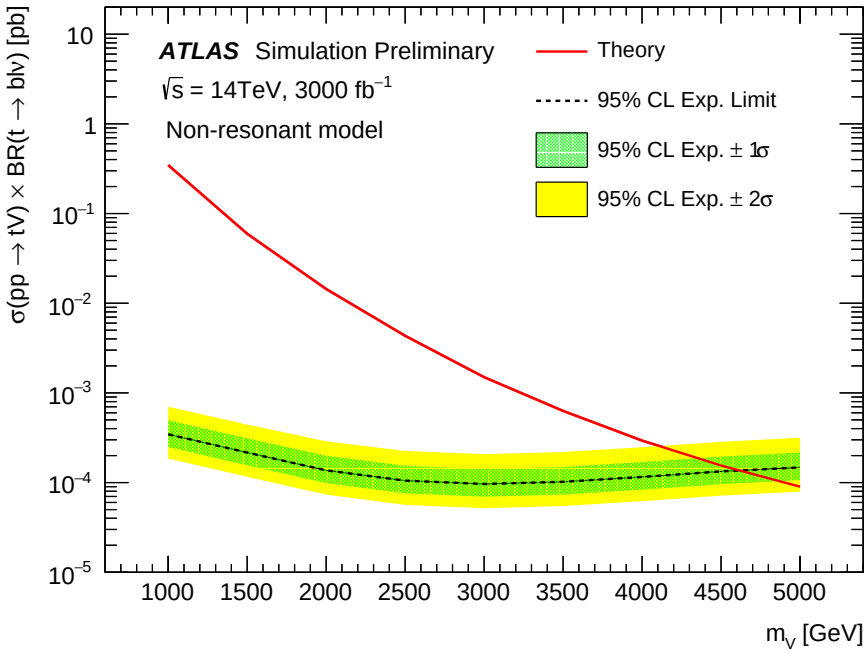

Figure 5: Expected 95% CLs upper limits on the signal cross-section as a function of the mass of the mediator for the non-resonant model assuming $m_\chi = 1$ GeV, $a = 0.5$ and $g_\chi = 1$ using a BDT analysis. The MC statistical uncertainty is not considered but the full set of systematics, extrapolated from the 13 TeVanalysis is considered.

The expectations for the equivalent of Run-3 integrated luminosity (300 fb^{-1}) is checked, obtaining an exclusion limit (discovery reach) of 3.7 TeV (3.2 TeV).

The expected mass limit at 95% CL obtained with the cut-based analysis, assuming an integrated luminosity of 3000 fb^{-1} and including same systematic uncertainties, is 3.2 TeV. As anticipated at the beginning of the section, this limit is significantly lower than what is obtained with the BDT-based analysis.

7 Conclusion

The expected sensitivity of a search for events with one top quark and large missing transverse momentum is estimated in pp collisions at a centre-of-mass energy of $\sqrt{s} = 14$ TeV with the ATLAS detector at the HL-LHC. A non-resonant production of an exotic state V, decaying to a pair of invisible dark-matter particles $\chi\bar{\chi}$, in association with a right-handed top quark is considered. Only the topologies where the W boson from the top quark decays into an electron or a muon and a neutrino are considered. The number of signal and background events are estimated from simulated truth particle-level information after applying smearing functions to mimic an upgraded ATLAS detector response in the HL-LHC environment. The expected exclusion limit at 95% CL on the mass of the exotic state V is, in the absence of MC statistical uncertainty but considering systematic uncertainties, 4.6 TeV using a multivariate analysis based on a

BDT and assuming an integrated luminosity of 3000 fb^{-1}. The discovery reach obtained is 4.0 TeV. If improvements in systematics would be translated in to a reduction of the uncertainties by a factor 2, the expected exclusion (discovery) would increase by 80 (50) GeV. Expected exclusion for Run-3 equivalent integrated luminosity (300 fb^{-1}) including systematics is 3.7 TeV, while the discovery reach is 3.2 TeV.

References

[1] ATLAS Collaboration, *Observation of a new particle in the search for the Standard Model Higgs boson with the ATLAS detector at the LHC*, Phys. Lett. B **716** (2012) 1, arXiv: 1207.7214 [hep-ex].

[2] CMS Collaboration, *Observation of a new boson at a mass of 125 GeV with the CMS experiment at the LHC*, Phys. Lett. B **716** (2012) 30, arXiv: 1207.7235 [hep-ex].

[3] V. Trimble, *Existence and Nature of Dark Matter in the Universe*, Ann. Rev. Astron. Astrophys. **25** (1987) 425.

[4] G. Bertone, D. Hooper and J. Silk, *Particle dark matter: Evidence, candidates and constraints*, Phys. Rept. **405** (2005) 279, arXiv: hep-ph/0404175 [hep-ph].

[5] J. L. Feng, *Dark Matter Candidates from Particle Physics and Methods of Detection*, Ann. Rev. Astron. Astrophys. **48** (2010) 495, arXiv: 1003.0904 [astro-ph.CO].

[6] ATLAS Collaboration, *Search for dark matter and other new phenomena in events with an energetic jet and large missing transverse momentum using the ATLAS detector*, JHEP **01** (2018) 126, arXiv: 1711.03301 [hep-ex].

[7] CMS Collaboration, *Search for dark matter produced with an energetic jet or a hadronically decaying W or Z boson at* $\sqrt{s} = 13$ *TeV*, JHEP **07** (2017) 014, arXiv: 1703.01651 [hep-ex].

[8] ATLAS Collaboration, *Search for dark matter produced in association with bottom or top quarks in* $\sqrt{s} = 13$ *TeV pp collisions with the ATLAS detector*, Eur. Phys. J. C **78** (2018) 18, arXiv: 1710.11412 [hep-ex].

[9] ATLAS Collaboration, *Search for top-squark pair production in final states with one lepton, jets, and missing transverse momentum using 36 fb*$^{-1}$ *of* $\sqrt{s} = 13$ *TeV pp collision data with the ATLAS detector*, JHEP **06** (2018) 108, arXiv: 1711.11520 [hep-ex].

[10] ATLAS Collaboration, *Search for dark matter at* $\sqrt{s} = 13$ *TeV in final states containing an energetic photon and large missing transverse momentum with the ATLAS detector*, Eur. Phys. J. C **77** (2017) 393, arXiv: 1704.03848 [hep-ex].

[11] CMS Collaboration, *Search for new physics in the monophoton final state in proton–proton collisions at* $\sqrt{s} = 13$ *TeV*, JHEP **10** (2017) 073, arXiv: 1706.03794 [hep-ex].

[12] ATLAS Collaboration, *Search for dark matter in events with a hadronically decaying vector boson and missing transverse momentum in pp collisions at* $\sqrt{s} = 13$ *TeV with the ATLAS detector*, 2018, arXiv: 1807.11471 [hep-ex].

[13] ATLAS Collaboration, *Search for an invisibly decaying Higgs boson or dark matter candidates produced in association with a Z boson in pp collisions at* $\sqrt{s} = 13$ *TeV with the ATLAS detector*, Phys. Lett. B **776** (2018) 318, arXiv: 1708.09624 [hep-ex].

[14] ATLAS Collaboration, *Search for Dark Matter Produced in Association with a Higgs Boson decaying to $b\bar{b}$ at $\sqrt{s}$ = 13 TeV with the ATLAS Detector using 79.8 fb^{-1} of proton-proton collision data*, ATLAS-CONF-2018-039, 2018, URL: http://cds.cern.ch/record/2632344.

[15] ATLAS Collaboration, *Search for dark matter in association with a Higgs boson decaying to two photons at $\sqrt{s}$ = 13 TeV with the ATLAS detector*, Phys. Rev. D **96** (2017) 112004, arXiv: 1706.03948 [hep-ex].

[16] CMS Collaboration, *Search for dark matter produced in association with a Higgs boson decaying to $\gamma\gamma$ or $\tau^+\tau^-$ at $\sqrt{s}$ = 13 TeV*, JHEP **09** (2018) 046, arXiv: 1806.04771 [hep-ex].

[17] CMS Collaboration, *Search for associated production of dark matter with a Higgs boson that decays to a pair of bottom quarks*, CMS-PAS-EXO-16-050, 2018, URL: https://cds.cern.ch/record/2628473.

[18] J. Andrea, B. Fuks and F. Maltoni, *Monotops at the LHC*, Phys. Rev. D **84** (2011) 074025, arXiv: 1106.6199 [hep-ph].

[19] D. Abercrombie et al., *Dark Matter Benchmark Models for Early LHC Run-2 Searches: Report of the ATLAS/CMS Dark Matter Forum*, 2015, arXiv: 1507.00966 [hep-ex].

[20] I. Boucheneb, G. Cacciapaglia, A. Deandrea and B. Fuks, *Revisiting monotop production at the LHC*, JHEP **01** (2015) 017, arXiv: 1407.7529 [hep-ph].

[21] ATLAS Collaboration, *Letter of Intent for the Phase-II Upgrade of the ATLAS Experiment*, CERN-LHCC-2012-022. LHCC-I-023, Draft version for comments, 2012, URL: https://cds.cern.ch/record/1502664.

[22] ATLAS Collaboration, *ATLAS Phase-II Upgrade Scoping Document*, CERN-LHCC-2015-020. LHCC-G-166, 2015, URL: https://cds.cern.ch/record/2055248.

[23] CDF Collaboration, *Search for a dark matter candidate produced in association with a single top quark in $p\bar{p}$ collisions at $\sqrt{s}$ = 1.96 TeV*, Phys. Rev. Lett. **108** (2012) 201802, arXiv: 1202.5653 [hep-ex].

[24] ATLAS Collaboration, *Search for invisible particles produced in association with single-top-quarks in proton–proton collisions at $\sqrt{s}$ = 8 TeV with the ATLAS detector*, Eur. Phys. J. C **75** (2015) 79, arXiv: 1410.5404 [hep-ex].

[25] CMS Collaboration, *Search for dark matter in events with energetic, hadronically decaying top quarks and missing transverse momentum at $\sqrt{s}$ = 13 TeV*, JHEP **06** (2018) 027, arXiv: 1801.08427 [hep-ex].

[26] CMS Collaboration, *Search for monotop signatures in proton–proton collisions at $\sqrt{s}$ = 8 TeV*, Phys. Rev. Lett. **114** (2015) 101801, arXiv: 1410.1149 [hep-ex].

[27] ATLAS Collaboration, *Technical Design Report for the ATLAS Inner Tracker Pixel Detector*, CERN-LHCC-2017-021. ATLAS-TDR-030, 2017, URL: https://cds.cern.ch/record/2285585.

[28] ATLAS Collaboration, *Technical Design Report for the ATLAS Inner Tracker Strip Detector*, CERN-LHCC-2017-005. ATLAS-TDR-025, 2017, URL: https://cds.cern.ch/record/2257755.

[29] ATLAS Collaboration, *Technical Design Report for the Phase-II Upgrade of the ATLAS LAr Calorimeter*, CERN-LHCC-2017-018. ATLAS-TDR-027, 2017, URL: https://cds.cern.ch/record/2285582.

[30] ATLAS Collaboration, *Technical Design Report for the Phase-II Upgrade of the ATLAS Tile Calorimeter*, CERN-LHCC-2017-019. ATLAS-TDR-028, 2017, URL: https://cds.cern.ch/record/2285583.

[31] ATLAS Collaboration, *A High-Granularity Timing Detector for ATLAS phase 2 upgrade: Initial Design Review document*, ATL-COM-LARG-2017-029, 2017, URL: https://cds.cern.ch/record/2276098.

[32] ATLAS Collaboration, *Technical Design Report for the Phase-II Upgrade of the ATLAS Muon Spectrometer*, CERN-LHCC-2017-017. ATLAS-TDR-026, 2017, URL: https://cds.cern.ch/record/2285580.

[33] ATLAS Collaboration, *Technical Design Report for the Phase-II Upgrade of the ATLAS TDAQ System*, CERN-LHCC-2017-020. ATLAS-TDR-029, 2017, URL: https://cds.cern.ch/record/2285584.

[34] ATLAS Collaboration, *Expected performance of the ATLAS detector at the HL-LHC*, IN PROGRESS, 2018.

[35] ATLAS Collaboration, *The ATLAS Simulation Infrastructure*, Eur. Phys. J. C **70** (2010) 823, arXiv: 1005.4568 [physics.ins-det].

[36] ATLAS Collaboration, *Expected pile-up values at the HL-LHC*, ATL-UPGRADE-PUB-2013-014, 2013, URL: https://cds.cern.ch/record/1604492.

[37] ATLAS Collaboration, *Expected performance for an upgraded ATLAS detector at High-Luminosity LHC*, ATL-PHYS-PUB-2016-026, 2016, URL: https://cds.cern.ch/record/2223839.

[38] ATLAS Collaboration, *Study on the prospects of a $t\bar{t}$ resonance search in events with one lepton at a High Luminosity LHC*, ATL-PHYS-PUB-2017-002, 2017, URL: https://cds.cern.ch/record/2243753.

[39] J. Alwall, R. Frederix, S. Frixione, V. Hirschi, F. Maltoni et al., *The automated computation of tree-level and next-to-leading order differential cross sections, and their matching to parton shower simulations*, JHEP **07** (2014) 079, arXiv: 1405.0301 [hep-ph].

[40] R. D. Ball et al., *Parton distributions for the LHC Run II*, JHEP **04** (2015) 040, arXiv: 1410.8849 [hep-ph].

[41] T. Sjöstrand et al., *An Introduction to PYTHIA 8.2*, Comput. Phys. Commun. **191** (2015) 159, arXiv: 1410.3012 [hep-ph].

[42] ATLAS Collaboration, *ATLAS Pythia 8 tunes to 7 TeV data*, ATL-PHYS-PUB-2014-021, 2014, URL: https://cds.cern.ch/record/1966419.

[43] R. D. Ball et al., *Parton distributions with LHC data*, Nucl. Phys. B **867** (2013) 244, arXiv: 1207.1303 [hep-ph].

[44] D. J. Lange, *The EvtGen particle decay simulation package*, Nucl. Instrum. Meth. A **462** (2001) 152.

[45] P. Nason, *A New method for combining NLO QCD with shower Monte Carlo algorithms*, JHEP **11** (2004) 040, arXiv: hep-ph/0409146.

[46] S. Frixione, P. Nason and C. Oleari, *Matching NLO QCD computations with Parton Shower simulations: the POWHEG method*, JHEP **11** (2007) 070, arXiv: 0709.2092 [hep-ph].

[47] S. Alioli, P. Nason, C. Oleari and E. Re, *A general framework for implementing NLO calculations in shower Monte Carlo programs: the POWHEG BOX*, JHEP **06** (2010) 043, arXiv: 1002.2581 [hep-ph].

[48] H.-L. Lai et al., *New parton distributions for collider physics*, Phys. Rev. D **82** (2010) 074024, arXiv: 1007.2241 [hep-ph].

[49] T. Sjöstrand, S. Mrenna and P. Z. Skands, *PYTHIA 6.4 Physics and Manual*, JHEP **05** (2006) 026, arXiv: hep-ph/0603175.

[50] P. Z. Skands, *Tuning Monte Carlo Generators: The Perugia Tunes*, Phys. Rev. D **82** (2010) 074018, arXiv: 1005.3457 [hep-ph].

[51] ATLAS Collaboration, *Measurement of the Z/γ^* boson transverse momentum distribution in pp collisions at $\sqrt{s}$ = 7 TeV with the ATLAS detector*, JHEP **09** (2014) 145, arXiv: 1406.3660 [hep-ex].

[52] N. Davidson, T. Przedzinski and Z. Was, *PHOTOS interface in C++: Technical and Physics Documentation*, Comput. Phys. Commun. **199** (2016) 86, arXiv: 1011.0937 [hep-ph].

[53] J. Pumplin et al., *New generation of parton distributions with uncertainties from global QCD analysis*, JHEP **07** (2002) 012, arXiv: hep-ph/0201195 [hep-ph].

[54] T. Gleisberg, S. Höche, F. Krauss, M. Schönherr, S. Schumann et al., *Event generation with SHERPA 1.1*, JHEP **02** (2009) 007, arXiv: 0811.4622 [hep-ph].

[55] M. Cacciari, G. P. Salam and G. Soyez, *The anti-k_t jet clustering algorithm*, JHEP **04** (2008) 063, arXiv: 0802.1189 [hep-ph].

[56] M. Cacciari, G. P. Salam and G. Soyez, *FastJet User Manual*, Eur. Phys. J. C **72** (2012) 1896, arXiv: 1111.6097 [hep-ph].

[57] ATLAS Collaboration, *Measurements of b-jet tagging efficiency with the ATLAS detector using $t\bar{t}$ events at $\sqrt{s}$ = 13 TeV*, JHEP **08** (2018) 089, arXiv: 1805.01845 [hep-ex].

[58] ATLAS Collaboration, *Optimisation of the ATLAS b-tagging performance for the 2016 LHC Run*, ATL-PHYS-PUB-2016-012, 2016, URL: https://cds.cern.ch/record/2160731.

[59] A. Hoecker et al., *TMVA - Toolkit for Multivariate Data Analysis*, 2007, arXiv: physics/0703039 [physics.data-an].

[60] G. Cowan, K. Cranmer, E. Gross and O. Vitells, *Asymptotic formulae for likelihood-based tests of new physics*, Eur. Phys. J. C **71** (2011) 1554, arXiv: 1007.1727 [physics.data-an], Erratum: Eur. Phys. J. C **73** (2013) 2501.